Carbohydrate Polymers 100 (2014) 31–39

Contents lists available at ScienceDirect

Carbohydrate Polymers

journal homepage: www.elsevier.com/locate/carbpol

Deformation micromechanics of all-cellulose nanocomposites: Comparing matrix and reinforcing components

Tanittha Pullawan[a], Arthur N. Wilkinson[b], Lina N. Zhang[c], Stephen J. Eichhorn[a,b,*]

[a] Materials Science Centre, School of Materials, University of Manchester, Grosvenor Street, Manchester M13 9PL, UK
[b] Northwest Composites Centre, School of Materials, University of Manchester, Sackville Street, Manchester M13 9PL, UK
[c] Department of Chemistry, Wuhan University, Wuhan 430072, People's Republic of China

ARTICLE INFO

Article history:
Received 16 July 2012
Received in revised form
21 November 2012
Accepted 14 December 2012
Available online 4 January 2013

Keywords:
Cellulose
Composite
Nanocrystals
Nanowhiskers

ABSTRACT

All-cellulose nanocomposites, comprising two different forms of cellulose nanowhiskers dispersed in two different matrix systems, are produced. Acid hydrolysis of both tunicate (T-CNWs) and cotton cellulose (CNWs) is carried out to produce the nanowhiskers. These nanowhiskers are then dispersed in a cellulose matrix material, produced using two dissolution methods; namely lithium chloride/N,N-dimethyl acetamide (LiCl/DMAc) and sodium hydroxide/urea (NaOH/urea). Crystallinity of both nanocomposite systems increases with the addition of nanowhiskers up to a volume fraction of 15 v/v%, after which a plateau is reached. Stress-transfer mechanisms, between the matrix and the nanowhiskers in both of these nanocomposites are reported. This is achieved by following both the mechanical deformation of the materials, and by following the molecular deformation of both the nanowhiskers and matrix phases using Raman spectroscopy. In order to carry out the latter of these analyses, two spectral peaks are used which correspond to different crystal allomorphs; cellulose-I for the nanowhiskers and cellulose-II for the matrix. It is shown that composites comprising a LiCl/DMAc based matrix perform better than NaOH/urea based systems, the T-CNWs provide better reinforcement than CNWs and that an optimum loading of nanowhiskers (at 15 v/v%) is required to obtain maximum tensile strength and modulus.

1. Introduction

Cellulose is the most "common organic polymer" and utilized material in the world (Klemm, Heublein, Fink, & Bohn, 2005). In recent years the use of cellulose nanofibres has been extensively reported in the literature as potential reinforcements in composite materials (Eichhorn, 2011; Eichhorn et al., 2010; Klemm et al., 2011). With relevance to the present work cellulose nanowhiskers were first discovered by Bengt Rånby in 1949 (Ranby, 1949). Later it was shown that these colloidal rod-like particles of cellulose could form stable chiral nematic liquid crystalline phases (Dong, Kimura, Revol, & Gray, 1996; Revol, Bradford, Giasson, Marchessault, & Gray, 1992).

Favier et al. in 1995 (Favier, Chanzy, & Cavaille, 1995) were the first to show that cellulose nanowhiskers could reinforce a polymer matrix material. Cellulose nanowhiskers have subsequently been reported to reinforce composite matrices such as epoxy resin (Tang & Weder, 2010), polyvinyl acetate (Rusli, Shanmuganathan, Rowan, Weder, & Eichhorn, 2010), polyurethane (Mendez et al., 2011) and polyesters (Goffin et al., 2011; Ten, Turtle, Bahr, Jiang, & Wolcott, 2010). Most recently they have been reported to reinforce hydrophobic polymers such as polypropylene (Pandey et al., 2012) and poly(styrene-co-butadiene) and polybutadiene (Dagnon, Shanmuganathan, Weder, & Rowan, 2012). In all of these nanocomposites, interfaces can occur between the nanowhiskers and the matrix, between the nanowhiskers themselves through hydrogen bonding in a paper-like network, or most probably via both mechanisms. Cellulose nanowhiskers and nanofibrils from tunicates are known to possess high stiffnesses; experimental values of ~140–150 GPa have been reported (Iwamoto, Kai, Isogai, & Iwata, 2009; Sturcova, Davies, & Eichhorn, 2005). This makes them ideal for reinforcement in composite matrices. It also is well-known that cellulose nanowhiskers can form percolated networks in nanocomposite materials above a certain volume fraction (Capadona, Shanmuganathan, Tyler, Rowan, & Weder, 2008; Capadona et al., 2007; Favier et al., 1995). It is these percolated networks that form the basis for much of the reinforcement observed in the nanocomposites, and disruption of the hydrogen bonding by water has shown that this effect can be "turned off", leading to a flexible material (Capadona et al., 2008; Rusli et al., 2010).

* Corresponding author. Present address: College of Engineering, Mathematics and Physical Sciences, University of Exeter, Physics Building, Stocker Road, Exeter EX4 4QL, UK. Tel.: +44 0 1392 72 5515; fax: +44 0 1392 217965.
E-mail address: s.j.eichhorn@exeter.ac.uk (S.J. Eichhorn).

0144-8617/$ – see front matter © 2013 Elsevier Ltd. All rights reserved.
http://dx.doi.org/10.1016/j.carbpol.2012.12.066

All-cellulose composites have been recently developed as an alternative to the conventional approach to natural fibre composites (Huber et al., 2012). They were first developed and called "all-cellulose" composites by Nishino et al. (Nishino, Matsuda, & Hirao, 2004). They can be made by combining cellulose fibres (in nano or micron sized form) with a dissolved matrix of the same material (Huber et al., 2012). This dissolved matrix can either be combined with the cellulose fibres (Qin, Soykeabkaew, Xiuyuan, & Peijs, 2008), or the outer perimeter of the fibres themselves can be selectively dissolved to form a matrix (Nishino & Arimoto, 2007; Soykeabkaew, Nishino, & Peijs, 2009a; Soykeabkaew, Sian, Gea, Nishino, & Peijs, 2009b). Nanosized fibres from bacterial (Soykeabkaew et al., 2009a,b), microcrystalline cellulose (Abbott & Bismarck, 2010; Gindl & Keckes, 2005) and cellulose nanowhiskers (Pullawan, Wilkinson, & Eichhorn, 2010; Qi, Cai, Zhang, & Kuga, 2009) have been reported as effective reinforcing agents for all-cellulose composites. In addition to this a number of cellulose dissolving solutions have been used to make the matrix component; these include lithium chloride/N,N-dimethyl acetamide (LiCl/DMAc) (Nishino et al., 2004), sodium hydroxide/urea (NaOH/urea) (Qi et al., 2009) and ionic liquids (Duchemin, Mathew, & Oksman, 2009; Ma, Zhou, Li, Li, & Ou, 2011; Ou et al., 2012; Yousefi, Nishino, Faezipour, Ebrahimi, & Shakeri, 2011; Zhao et al., 2009). Of these solvent systems, NaOH/urea has been recently reported as a promising approach for the dissolution of cellulose for a variety of applications, including all-cellulose composites (Cai & Zhang, 2005, 2006; Cai et al., 2007; Zhou & Zhang, 2000).

It has been reported that enhanced mechanical properties are obtained for all-cellulose composites compared to conventional natural plant fibre-based composites (Huber et al., 2012). It is therefore important to better understand the interfaces that lead to these enhanced effects seen in these so-called "interface-less" composites (Huber et al., 2012). Some work has already been carried out to monitor interfaces in all-cellulose composites, both using X-ray diffraction (Gindl, Martinschitz, Boesecke, & Keckes, 2006) and Raman spectroscopy (Pullawan et al., 2010; Pullawan, Wilkinson, & Eichhorn, 2012).

The Raman spectroscopic method for analysing interfaces in composites relies on the monitoring of a shift in the peak position of a characteristic Raman band. This band is typically associated with the main-chain or backbone moieties of the polymer as the material is deformed, either in tension or compression. The effect was first observed for cellulose in 1997 (Hamad & Eichhorn, 1997), and has subsequently been applied to a wide range of fibres (Eichhorn & Young, 2001; Eichhorn, Hughes, Snell, & Mott, 2000; Eichhorn, Sirichaisit, & Young, 2001a; Eichhorn, Young, & Yeh, 2001b; Gierlinger, Schwanninger, Reinecke, & Burgert, 2006; Hamad, Gurnagul, & Gulati, 2012; Peetla, Schenzel, & Diepenbrock, 2006), cellulose fibre reinforced composite materials (Eichhorn & Young, 2003, 2004; Mottershead & Eichhorn, 2007; Tze, O'Neill, Tripp, Gardner, & Shaler, 2007) and most recently cellulose nanofibres and composites (Rusli & Eichhorn, 2008, 2011; Rusli et al., 2010; Rusli, Shanmuganathan, Rowan, Weder, & Eichhorn, 2011).

In the present work we explore the influence of both the reinforcement type (cellulose nanowhiskers from tunicates and cotton) and the matrix type (dissolved cellulose using LiCl/DMAc and NaOH/urea) on the stress transfer properties of all-cellulose nanocomposites.

2. Experimental methods

2.1. Materials

Acetic acid, sodium hypochlorite solution (>4% chlorine) and sulphuric acid (98%) were all purchased from Fisher Scientific. Lithium chloride (LiCl) and N,N-dimethylacetamide (DMAc) were purchased from Sigma–Aldrich. Microcrystalline cellulose (Avicell, PH-101, particle size ~50 μm) was also purchased from Sigma–Aldrich. Ion exchange resin (Amberlite MB 6113) was purchased from Fluka.

2.2. Production of cellulose nanowhiskers

Tunicate cellulose nanowhiskers (T-CNWs) were prepared by acid hydrolysis of tunicates (*Styela clava*) using sulphuric acid. The tunicates were first gutted and then heated in 3% (w/w) aqueous potassium hydroxide at 80 °C for 24 h in order to remove their outer walls, followed by mechanical agitation and scrubbing (van den Berg, Capadona, & Weder, 2007). Two more treatments with aqueous potassium hydroxide are then required, which is a slight modification of a procedure previously reported by Yuan, Nishiyama, Wada, & Kuga (2006). After neutralizing the tunicates with 3 L of water, 5 ml of acetic acid and 10 ml of sodium hypochlorite solution were added and heated up to 60 °C for 1 h. After this, 5 ml of acetic acid and 10 ml of sodium hypochlorite solution were added until the tunicate's colour changed to pure white. This bleaching procedure was repeated 2–3 times, depending on the particular batch of tunicates. These bleached deproteinised walls were then washed with de-ionised water and disintegrated using a Warring blender to yield a fine cellulose pulp. Sulphate-functionalised tunicate nanowhiskers were then prepared by sulphuric acid hydrolysis of tunicates according to a modification of a method described by Elazzouzi-Hafraoui et al. (2008). The fine cellulose pulp was added to 48% sulphuric acid and subjected to vigorous mechanical stirring. The suspension was then heated to 55 °C for 13 h while continually stirring. The dispersion was then cooled, filtered and washed with de-ionised water until a neutral pH was reached. These nanowhiskers were then re-dispersed in 1 L of de-ionised water, sonicated overnight and freeze-dried.

Cotton cellulose nanowhiskers (CNWs) were prepared using a standard sulphuric acid hydrolysis of cotton linters as described by Revol et al. (1992). A graduated cylinder containing 64% (w/w) sulphuric acid was placed into a water bath at 45 °C. The cotton linters (40 g) were then added to the acid and stirred mechanically for 45 min. De-ionised water (2.5 L) was then used to dilute this suspension, which was then settled and rinsed by centrifugation for 4 cycles (Centrifugation Sigma U-16, Sci-Quip) at 6000 rpm, using 10 min for each cycle. This suspension was then dialysed against water until neutralized. After treatment with an ion-exchange resin it was filtered using Whatman microfibre filters. The suspension was then repeatedly sonicated (Branson Digital Sonifier) to produce a colloidal suspension of nanowhiskers. This suspension was then freeze-dried.

2.3. Production of all-cellulose nanocomposites

All-cellulose nanocomposite films were prepared using a matrix of cellulose derived using two different solvent systems; namely lithium chloride/N,N-dimethyl acetamide (LiCl/DMAc) and sodium hydroxide/urea (NaOH/urea). These two different matrices required two very different processing routes. For the LiCl/DMAc system the first stage microcrystalline cellulose was "activated" in de-ionised water for 5 h at room temperature. This step swells the cellulose in preparation for dissolution. This activated cellulose was then dehydrated in acetone and then in N,N-dimethylacetamide (DMAc) for 5 h and 4 h, respectively. Following this, the DMAc was decanted from the dehydrated cellulose. An 8% solution (by total weight) of LiCl was then added to the DMAc; 8 g of LiCl in 100 g of DMAc. This solution was stirred at 120 °C for 30 min until the LiCl had completely dissolved. This solution was then added to

the cellulose, stirred using a magnetic stirrer, at room temperature for 5–10 min. The resultant solution was stored in a sealed bottle for 1 week to allow the dissolution to continue. The final cellulose solution was centrifuged at 6000 rpm for 5 min to remove any air bubbles and allow any large undissolved cellulose particles to sediment. The presence of these particles was however found to be in significant.

In order to prepare the NaOH/urea solvent dissolved cellulose a 100 g mixture of NaOH, urea and de-ionised water, in weight proportions, was prepared. This mixture was pre-cooled to ~13 °C. Cotton linters (5 g of pulp) were added to this mixture and vigorously stirred for 5 min to obtain a transparent solution. It was found that it was not possible to use activated microcrystalline cellulose as a starting material for this solvent system. The solution, having dissolved the cellulose, was then centrifuged at 6000 rpm for 10 min to remove any air bubbles.

T-CNWs and CNWs were separately added to these two matrix systems using two slightly different methods, but varying the nanowhisker content from 5 to 20% (prepared from 10 wt% T-CNWs and CNWs suspensions). For the LiCl/DMAc system nanowhiskers were simply added to the solution and ultrasonicated for 6 h. For the NaOH/urea system the suspension was warmed to room temperature and the nanowhiskers were added and stirred for 30 min. After this the suspension was centrifuged at 6000 rpm for 5 min. In each case a transparent suspension resulted. The LiCl/DMAc/nanowhiskers suspension was cast into a Petri dish and left under ambient conditions until a transparent film formed. This film was then washed in de-ionised water to remove any residual solvent and dried on a glass plate under ambient temperature conditions. The NaOH/urea/nanowhiskers suspension was spread on a glass plate which was then immersed in a coagulation bath of 5 wt% sulphuric acid for 5 min at room temperature. The final film thicknesses were in the range 30–50 μm.

2.4. X-ray diffraction of all-cellulose nanocomposites

The crystallinities of the all-cellulose nanocomposites were determined using an X-ray diffractometer (Phillips X'Pert-MPD) using 1.54 Å CuKα radiation, with a step size of 0.05° over the 2θ range 5–60°. Segal's method (Segal, Creely, Martin, & Conrad, 1959) was used to determine the percentage crystallinity (χ) according to the equation

$$\chi = \frac{I_{200} - I_{am}}{I_{200}} \times 100 \quad (1)$$

where I_{200} is the maximum intensity of the 2 0 0 lattice reflection, which is typically located in the range 2θ = 21–23° for cellulose, and I_{am} is the intensity of the region of the diffraction pattern located at 2θ = 18°; the location of the intensity maxima for fully amorphous cellulose. Samples were rotated in the diffractometer to overcome effects of preferred orientation. The films do not contain oriented nanowhiskers, as has previously been reported (Pullawan et al., 2012).

2.5. Mechanical testing of all-cellulose nanocomposites

The all-cellulose nanocomposite films were cut into 50 mm × 5 mm strips. The thicknesses of these strips were determined using a micrometre. Prior to testing all samples were equilibrated at a temperature and humidity of 23 ± 1 °C and 50 ± 5% for 24 h. The tensile properties of the composite films were obtained using an Instron 1121 universal testing machine with Series IX software. After calibrating the machine, samples were mounted between the grips and deformed in tension at a cross-head speed of 1 mm min^{-1}. A load cell (full-scale of 500 N) was used to record the load and at least 10 samples were tested to failure for each volume fraction. Strain was assumed to be the equal to the cross-head displacement divided by the original length of the sample. Engineering stress was determined by dividing the load by the cross-sectional area of the sample.

2.6. Raman spectroscopy and micromechanics of all-cellulose nanocomposites

A Renishaw system 1000 Raman imaging microscope with a low power (25 mW) near infrared laser (785 nm) was used to record spectra from the all-cellulose nanocomposites. A 50× objective lens with a 0.60 numerical aperture was used to focus the laser on the samples to a spot size of ~1–2 μm. Spectra were recorded in the range 1060–1140 cm^{-1}, including an intense peak located at ~1095 cm^{-1}. A similar spectral range was also captured to record the position of a peak located at ~895 cm^{-1}. All spectra were recorded using an exposure time of 40 s with 4 accumulations. The laser polarization direction was set to be parallel to the deformation axis of the samples and the scattered light was also polarized in the same direction. Samples were deformed in tension using a Deben Microtest deformation rig. Each sample was secured to a cardboard 'window' specimen mount, which was clamped between the jaws of the rig. Each side of the card was burnt away using an artists' pyrography machine. Tensile increments (0.2%) were applied to the specimen and at each increment a Raman spectrum was recorded. Each spectrum was fitted, in order to find the peak positions, using an automated algorithm, and a mixed Gaussian–Lorentzian function, based on the work of Marquardt (1963).

3. Results and discussion

3.1. X-ray diffraction and crystallinity

Typical X-ray diffraction patterns obtained from both pure matrix materials (LiCl/DMAc and NaOH/urea dissolved cellulose) and nanocomposite specimens containing nanowhiskers (T-CNWs and CNWs; both at 20 v/v%) are shown in Fig. 1a and b. All peaks for the LiCl/DMAc solvent derived matrix material (Fig. 1a) are indicative of a cellulose-II structure. The peaks present for the NaOH/urea are also indicative of a cellulose-II structure; with the exception of a peak located just to the left of the cellulose peak at ~11.9° which is thought to be due to the silicone adhesive used to secure the samples to the stage. This peak is not as intense for the LiCl/DMAc samples. We have previously noted its appearance (Pullawan et al., 2010) but also note that it does not affect the measurement of crystallinity using Segal's method. Other peaks located at 2θ = 12.1, 19.8, and 22.0° are characteristic of the (1 $\bar{1}$ 0), (1 1 0) and (2 0 0) planes assigned to the cellulose-II crystal, in agreement with Qi et al. (2009). The shapes of the peaks located at 2θ = 21–23° are unique for the different solvent systems. This may be due to the fact that different starting materials were used resulting in different crystal sizes in the regenerated cellulose. The shape and form of the peak located at ~22°, assigned to the (2 0 0) plane by Abbott & Bismarck (2010), has the suggestion of a slight shoulder on its left side, hence our assignment of (1 1 0)/(2 0 0). When the cellulose nanowhiskers are added to these matrix materials (Fig. 1b) again unique diffraction patterns are observed for the two different matrix systems. The LiCl/DMAc system exhibits a much broader peak at 2θ = 21–23°, which would suggest a smaller lateral crystal size. No apparent differences are observed between diffraction patterns for nanocomposites with different nanowhisker types contained within the same matrix systems.

The crystallinities of the samples as a function of volume fraction of nanowhiskers are reported in Fig. 2a and b for the two matrix systems, and compared with the pure nanowhiskers. The T-CNWs

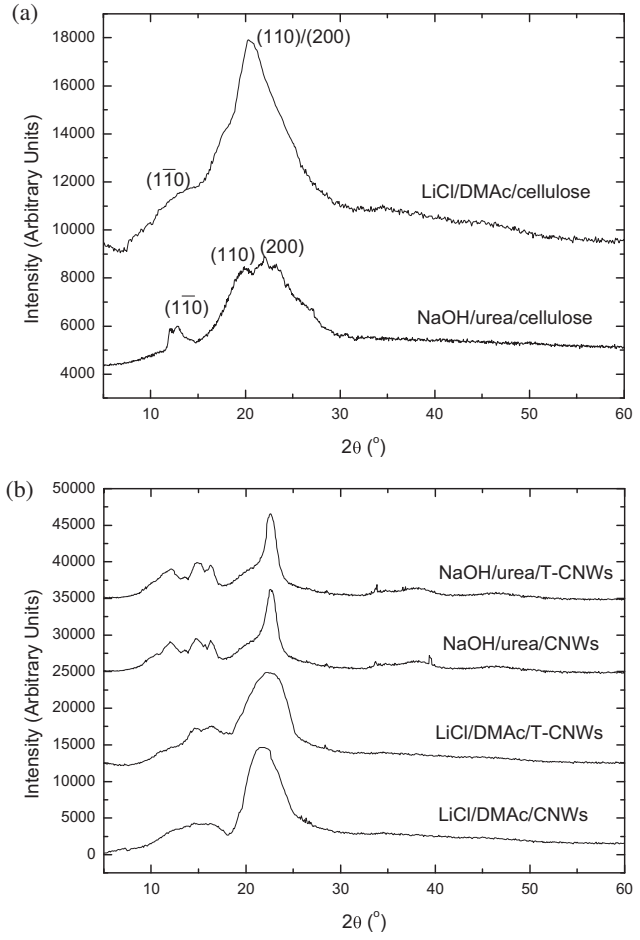

Fig. 1. Typical X-ray diffraction patterns for (a) pure cellulose matrix systems derived using LiCl/DMAc and NaOH/urea solvent systems and (b) all-cellulose nanocomposites produced using these matrix systems and containing cellulose nanowhiskers derived from tunicates (T-CNWs) and cotton (CNWs). Whisker content 15 v/v%.

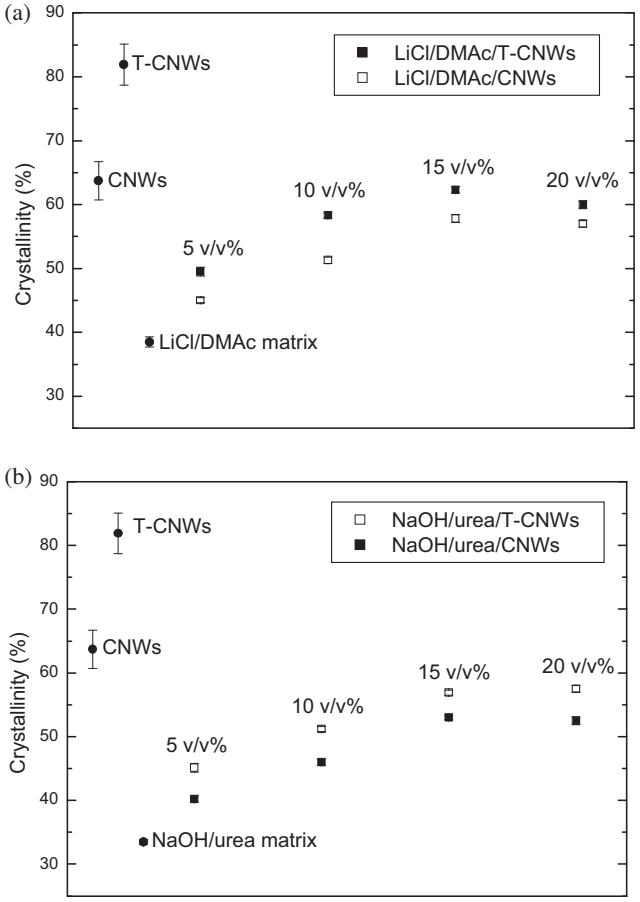

Fig. 2. Crystallinities of cellulose nanowhiskers, matrix systems and all-cellulose nanocomposites; (a) all-cellulose nanocomposites produced using a LiCl/DMAc solvent system compared to cellulose nanowhiskers from tunicate (T-CNWs) and cotton (CNWs) and a pure matrix system (LiCl/DMAc matrix) and (b) all-cellulose nanocomposites produced using a NaOH/urea solvent system compared to cellulose nanowhiskers from tunicate (T-CNWs) and cotton (CNWs) and a pure matrix system (NaOH/urea matrix).

have a much higher crystallinity (>80%) than the CNWs. This is possibly as a result of the higher crystallinity of the cellulose in the starting material. Conversely, the crystallinities of both pure matrix systems are low (<40%), with the LiCl/DMAc system yielding a slightly higher crystallinity than the NaOH/urea system. The crystallinities of the nanocomposites also increase with the addition of nanowhiskers, up to a maximum at 15 v/v%. The samples containing T-CNWs have marginally higher overall crystallinities, for both matrix systems, than for CNWs; this is thought to be simply due to the higher crystallinity of the T-CNWs. Above 15 v/v% of nanowhiskers the crystallinity is observed to plateau, within the margins of error.

3.2. Mechanical properties of all-cellulose nanocomposites

Typical stress strain curves for nanocomposites containing varying volume fractions of T-CNWs and CNWs, for both matrix systems are shown in Fig. 3. All curves are non-linear, with an initial steep slope, and a yield point at ~1%. Yield points of ~1% have been previously observed, and commented, on for regenerated cellulose fibres (Kong & Eichhorn, 2005a,b). Here it was shown from spectroscopic data that a breakdown of hydrogen bonding occurs at this point (Kong & Eichhorn, 2005b), but evidence for this was not obtained for these samples. Nevertheless, hydrogen bonding between the matrix and the reinforcing nanowhiskers, and also within the networks of nanowhiskers themselves, is thought to play a significant role in the mechanics of these materials. The shape of this curve is also typical for cellulose-based self-reinforced films previously reported in the literature (Gindl & Keckes, 2007). The change in slope for these materials was reported to be due to a disruption of intramolecular and intermolecular hydrogen bonds (Gindl & Keckes, 2007). Given the high volume fractions of nanowhiskers present in our nanocomposites it is thought that we are above the percolation threshold. The aspect ratios of our nanowhiskers are 72.8 ± 40.8 and 17.2 ± 6.2 for T-CNWs and CNWs respectively, as previously reported (Pullawan et al., 2012). This means that the critical concentrations for percolation C_V given by the equation (Capadona et al., 2008).

$$C_V = \frac{0.7}{A} \quad (2)$$

are ~1% and ~4%. We accept there is a lot of heterogenaiety to the aspect ratio data but in each case with the very lowest aspect ratio possible this leads to values of ~2% and ~6%. Therefore all of our samples are thought to be above the percolation threshold concentration. This means that hydrogen bonding should definitely play a significant role in the mechanics of these materials. Any enhancement of this bonding could therefore be a possible route to improve mechanical properties.

For the LiCl/DMAc system, the tensile strength increased considerably with respect to the matrix film, and reached maximum values of 165.4 ± 3.9 MPa and 142.5 ± 4.1 MPa for 15 v/v% of

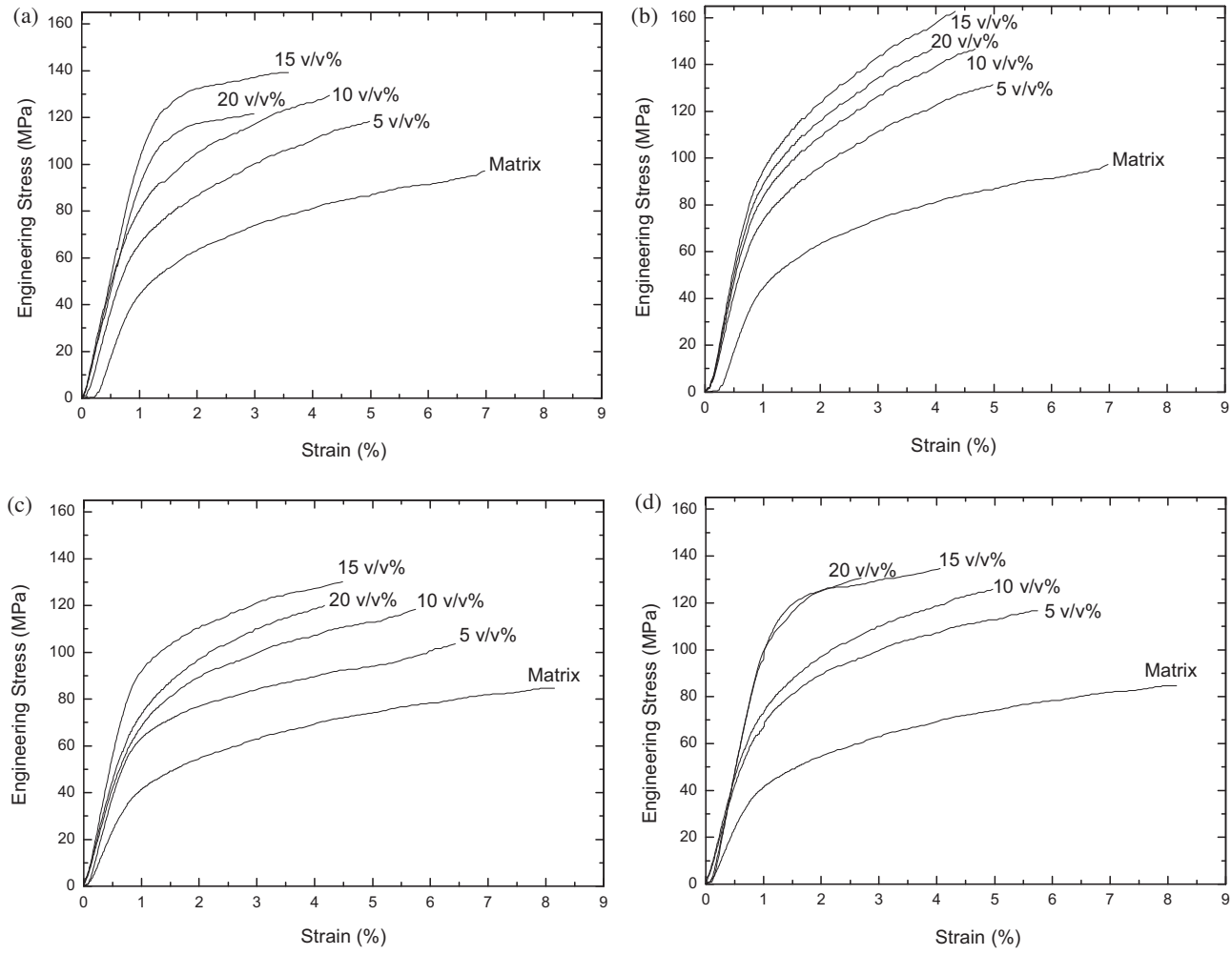

Fig. 3. Typical stress strain curves for pure cellulose matrices and all-cellulose nanocomposites produced using a LiCl/DMAc solvent system (a and b) and an NaOH/urea solvent system (c and d), reinforced using cellulose nanowhiskers derived from (a and c) tunicates (T-CNWs) and (b and d) cotton (CNWs) at a range of volume fractions (5–20 v/v%).

T-CNWs and CNWs respectively (see Table 1 and Fig. 3a and b). Young's moduli of the nanocomposites also increased with the addition of nanowhiskers; 293% and 183% for T-CNWs and CNWs respectively (up to 15 v/v%; see Table 1). In a similar manner the maximum tensile strength of nanocomposites produced using a NaOH/urea solvent system also increases with increasing whisker content up to a maximum at 15 v/v%; to 137.1 ± 2.9 MPa and 127.4 ± 3.7 MPa for T-CNWs and CNWs respectively (see Table 2 and Fig. 3c and d). Young's moduli also increase, up to a maximum at the same volume fraction; by 312% and 192% for T-CNWs and CNWs respectively (see Table 2). These increases are thought to occur due to the increasing influence of the stiff nanowhiskers, and the stress transfer between the matrix and this phase. As the whisker content increases, the strain to failure of the nanocomposites decreases, leading to an embrittlement of the material. A decrease in mechanical properties is noted at higher concentrations for all nanocomposite samples, with one exception, where the modulus of the NaOH/urea/T-CNWs sample at 20 v/v% appears to be the same (within error bounds) as the 15 v/v% sample. The mechanical properties of our films are comparable to other

Table 1
Mechanical properties for pure matrix material and all-cellulose nanocomposites produced using an LiCl/DMAc solvent system and a range of volume fractions (5–20 v/v%) of cellulose nanowhiskers derived from tunicates (T-CNWs) and cotton (CNWs).

Sample	Young's modulus (GPa)	Stress at break (MPa)	Strain at break (%)
Matrix film	3.0 ± 0.1	97.7 ± 3.9	7.3 ± 0.3
5 v/v% CNWs	5.1 ± 0.4	118.4 ± 3.5	4.7 ± 0.2
10 v/v%CNWs	6.3 ± 0.3	132.1 ± 4.0	4.0 ± 0.2
15 v/v%CNWs	8.0 ± 0.2	142.5 ± 4.1	3.4 ± 0.2
20 v/v%CNWs	8.5 ± 0.2	126.9 ± 3.8	2.8 ± 0.3
5 v/v%TNWs	6.3 ± 0.3	134.0 ± 4.2	4.4 ± 0.5
10 v/v%TNWs	8.1 ± 0.1	149.2 ± 3.2	3.8 ± 0.4
15 v/v%TNWs	11.8 ± 0.2	165.4 ± 3.9	3.2 ± 0.6
20 v/v%TNWs	12.0 ± 0.2	153.4 ± 3.0	2.8 ± 0.6

Table 2
Mechanical properties for pure matrix material and all-cellulose nanocomposites produced using an NaOH/urea solvent system and a range of volume fractions (5–20 v/v%) of cellulose nanowhiskers derived from tunicates (T-CNWs) and cotton (CNWs).

Sample	Young's modulus (GPa)	Stress at break (MPa)	Strain at break (%)
Matrix film	2.5 ± 0.2	81.4 ± 3.9	7.8 ± 0.3
5 v/v% CNWs	4.5 ± 0.2	103.6 ± 2.2	6.4 ± 0.4
10 v/v% CNWs	5.5 ± 0.1	119.6 ± 2.1	5.2 ± 0.3
15 v/v% CNWs	7.2 ± 0.1	127.4 ± 3.7	4.3 ± 0.2
20 v/v% CNWs	7.3 ± 0.2	124.4 ± 2.8	3.8 ± 0.2
5 v/v% TNWs	5.8 ± 0.2	116.2 ± 3.0	5.7 ± 0.3
10 v/v% TNWs	8.0 ± 0.2	128.2 ± 3.5	4.9 ± 0.2
15 v/v% TNWs	9.8 ± 0.2	137.1 ± 2.9	4.1 ± 0.2
20 v/v% TNWs	10.3 ± 0.2	133.0 ± 2.8	2.7 ± 0.3

all-cellulose nanocomposites reinforced with nanowhiskers reported in the literature *e.g.* 124 MPa for strength and 5.1 GPa modulus (at 10 v/v%) (Qi et al., 2009). They are however lower than unidirectionally oriented all-cellulose composites, where typically values of ~400–900 MPa and ~20–30 GPa for strength and modulus have been reported (Soykeabkaew et al., 2009a,b; Gindl et al., 2006; Nishino et al., 2004).

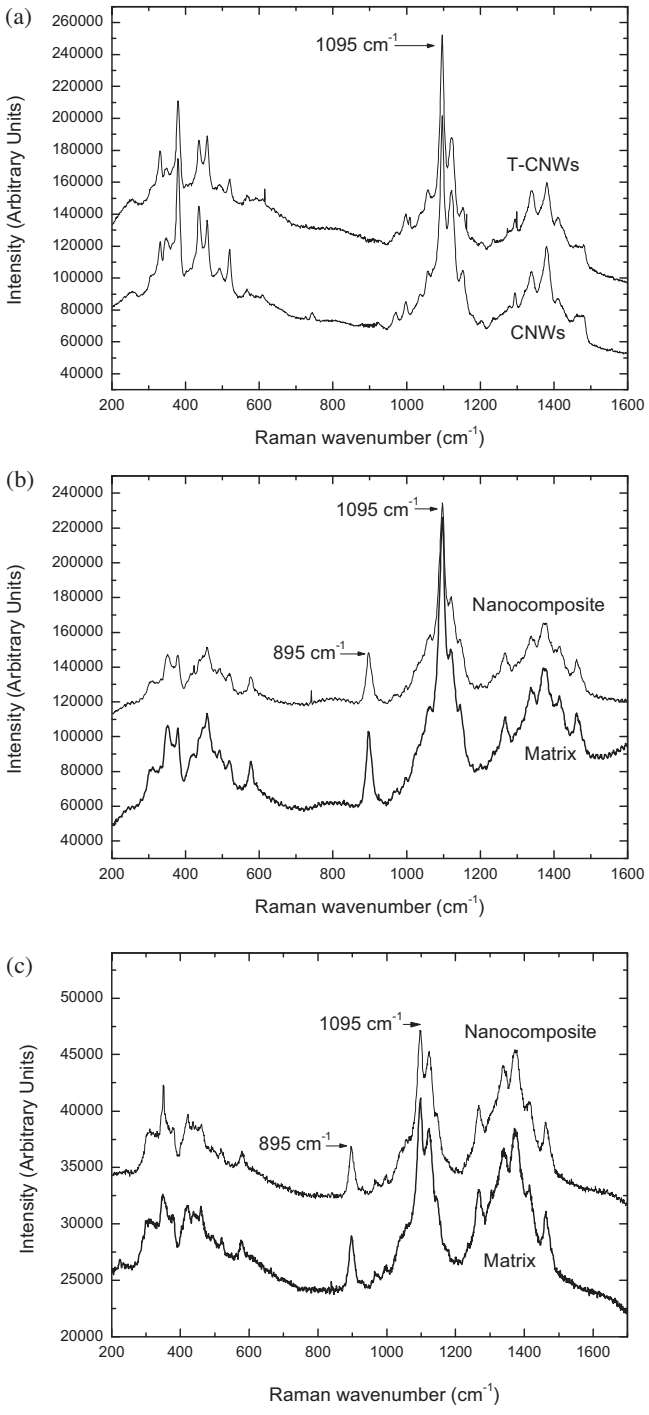

Fig. 4. Typical Raman spectra obtained in the range 200–1600 cm^{-1} for (a) cellulose nanowhiskers derived from tunicates (T-CNWs) and cotton (CNWs) highlighting the position of a band located at ~1095 cm^{-1}, (b) an all-cellulose nanocomposite comprising cellulose nanowhiskers (T-CNWs) contained in a cellulose matrix derived from an LiCl/DMAc solvent system and the pure matrix system without nanowhiskers and (c) an all-cellulose nanocomposite comprising cellulose nanowhiskers (T-CNWs) contained in a cellulose matrix derived from an NaOH/urea solvent system and the pure matrix system without nanowhiskers.

3.3. Micromechanical properties of all-cellulose nanocomposites

Well-defined Raman spectra are obtained from the nanowhiskers (T-CNWs, CNWs), the matrices (from LiCl/DMAc and NaOH/urea solvent systems) and the nanocomposites comprising these components (see Fig. 4). The most prominent peak in the spectra obtained from all samples is located at ~1095 cm^{-1}. This peak has been previously assigned to the C—O stretch modes along the cellulose backbone (Wiley & Atalla, 1987) and most recently to the glycosidic moiety (—C—O—C—) (Gierlinger et al., 2006). There are no observable differences in the Raman spectra for T-CNWs and CNWs (see Fig. 4a), and each spectrum is indicative of a cellulose-I allomorph (Wiley & Atalla, 1987). The Raman spectrum for cellulose-II is differentiated from that of cellulose-I by the presence of a peak located at ~895 cm^{-1}; this peak is clearly observed for both matrix systems (see Fig. 4b and c) (Atalla & Dimick, 1975). This indicates that the NaOH/urea solvent system does produce a cellulose-II allomorph of cellulose. When the nanowhiskers are added to each matrix system a composite spectrum is obtained, with the peak located at ~1095 cm^{-1} comprising signals from both the reinforcing nanowhiskers and the matrix. The peak located at ~895 cm^{-1} is thought to be only due to the matrix phase, and can be used to discriminate the deformation of this phase from the reinforcing whiskers (Pullawan et al., 2010). The Raman band initially located at ~1095 cm^{-1} is much lower in intensity for

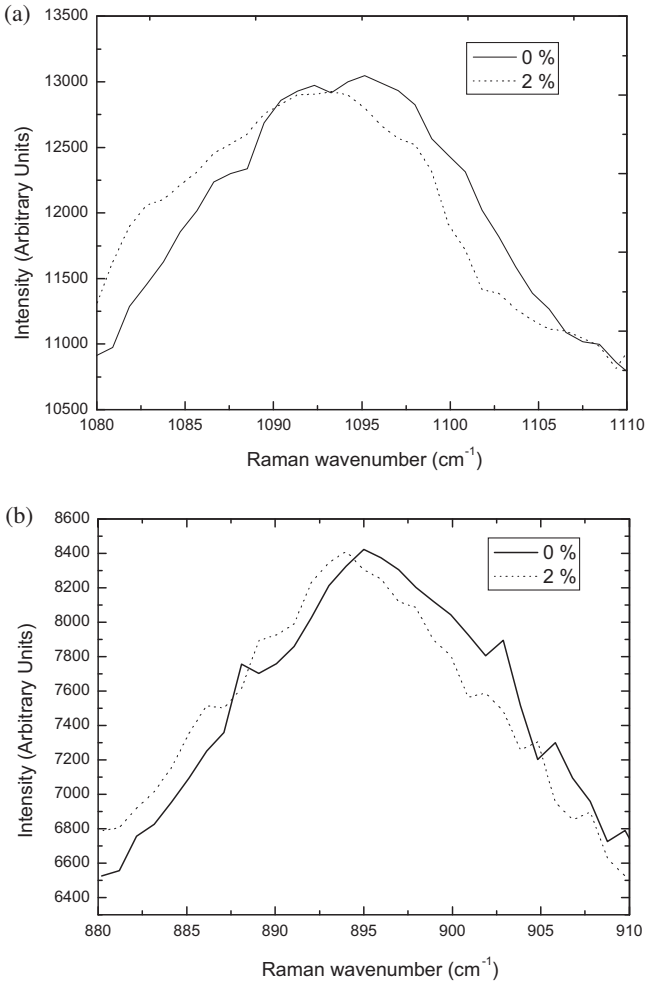

Fig. 5. Typical shifts in the peak positions for Raman bands initially located at (a) ~1095 cm^{-1} and (b) ~ 895 cm^{-1} for all-cellulose nanocomposites produced using a LiCl/DMAc solvent system derived matrix reinforced with 15 v/v% tunicate cellulose nanowhiskers (T-CNWs).

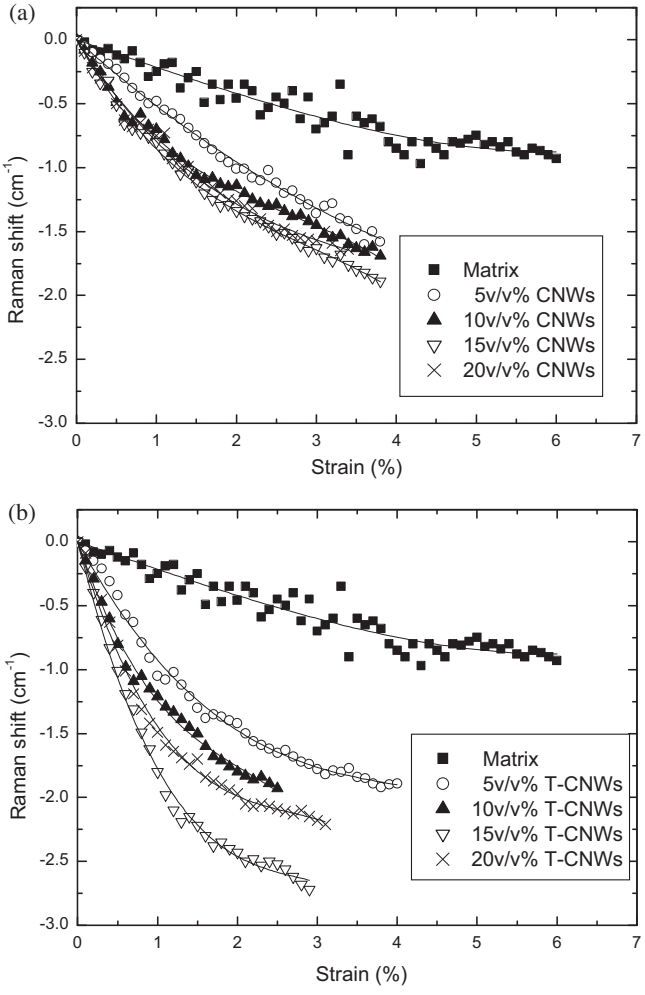

Fig. 6. Shifts in the peak positions of the Raman band initially located at ~1095 cm^{-1} as a function of tensile deformation of all-cellulose nanocomposites and matrix materials produced using a LiCl/DMAc solvent system reinforced with cellulose nanowhiskers derived from (a) tunicates (T-CNWs) and (b) cotton (CNWs) with a range of volume fractions (5–20 v/v%).

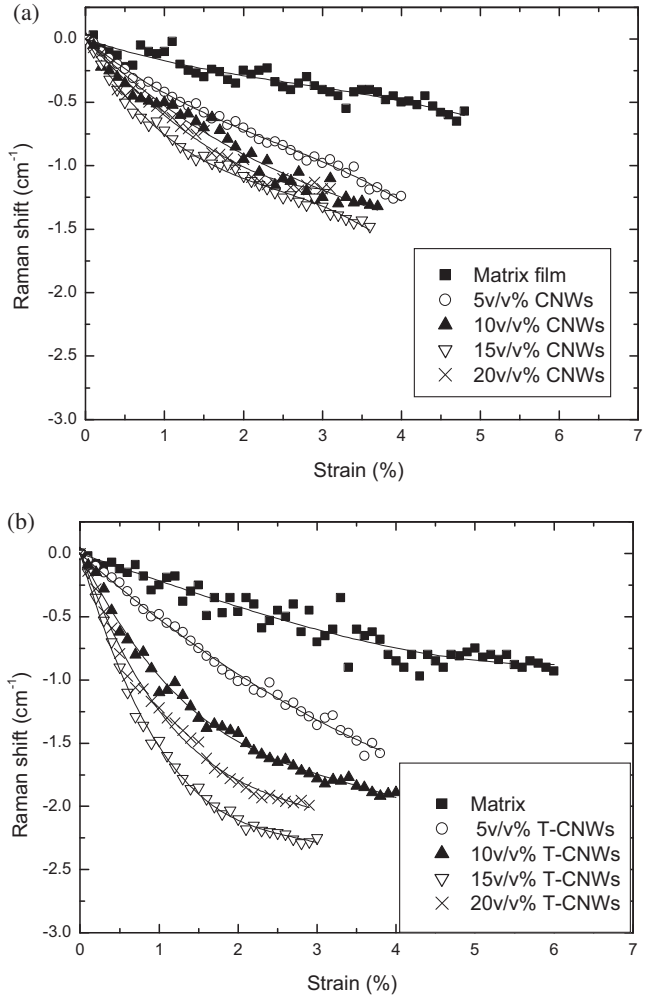

Fig. 7. Shifts in the peak positions of the Raman band initially located at ~1095 cm^{-1} as a function of tensile deformation of all-cellulose nanocomposites and matrix materials produced using an NaOH/urea solvent system reinforced with cellulose nanowhiskers derived from (a) tunicates (T-CNWs) and (b) cotton (CNWs) with a range of volume fractions (5–20 v/v%). Solid lines are 3rd order polynomial fits to the data.

the NaOH/urea sample than for the LiCl/DMAc sample, possibly suggesting a slightly different form to the matrix.

Both the bands located at ~1095 cm^{-1} and ~895 cm^{-1} were found to shift towards a lower wavenumber position, upon the application of tensile deformation; typical examples of this are shown in Fig. 5a and b. These shifts are indicative of molecular deformation of the cellulose chains within the nanocomposites arising due to stress-transfer within each component; namely the reinforcing nanowhiskers and the matrix. Detailed positional data from both bands for nanocomposites comprising two different forms of cellulose nanowhiskers and the two matrix systems are reported in Figs. 6 and 7. These data indicate a non-linear shift in wavenumber position, reflecting the shape of the stress-strain curves shown in Fig. 3. These data all show that as the volume fraction of the nanowhiskers is increased, the rates of the shifts with respect to strain appear to increase. This increase can be attributed to an increasing stiffness of the composites, due to the presence of increasing volume fractions of nanowhiskers; since the band shift rate with respect to strain has previously been shown to be proportional to the modulus (Eichhorn et al., 2001a,b). It is noticeable however that above 15 v/v% the shift rate of the data (for the 20 v/v%) appears to decrease. This is in agreement with the mechanical properties and crystallinity data (see Tables 1 and 2). Qualitatively it is also noted that the data for the nanocomposites using a NaOH/urea system appear to be overlap to a greater extent than the LiCl/DMAc based samples. Much lower increases in mechanical properties are noted for the NaOH/urea matrix system-based nanocomposites.

During deformation of the samples, the position of the Raman band initially located at ~895 cm^{-1} was also recorded. These data are reported in Fig. 8a and b for the LiCl/DMAc and NaOH/urea matrix based nanocomposites. For brevity we only show data from the 15 v/v% samples, as these were expected to show the greatest difference compared to the unreinforced matrix. Little difference is however observed between datasets; matrix and 15 v/v% samples' datasets almost overlap. This shows that the mechanical properties of the nanocomposites are mostly dictated by the presence of the nanowhisker phase, and little effect is noted in the matrix itself. This is what would be expected for a typical composite material.

All shift data (Figs. 6 and 7) have been fitted using 3rd order polynomials. By taking the first derivative of this fit, the gradients of these curve have been obtained. This calculation was performed at a strain of 0.5%, and these data are reported in Tables 3 and 4. No clear differences can be seen between the shift rates with respect to strain for the pure matrix materials. On average the shift rates observed for the nanocomposites made with the LiCl/DMAc matrix system are higher than those made with the NaOH/urea system,

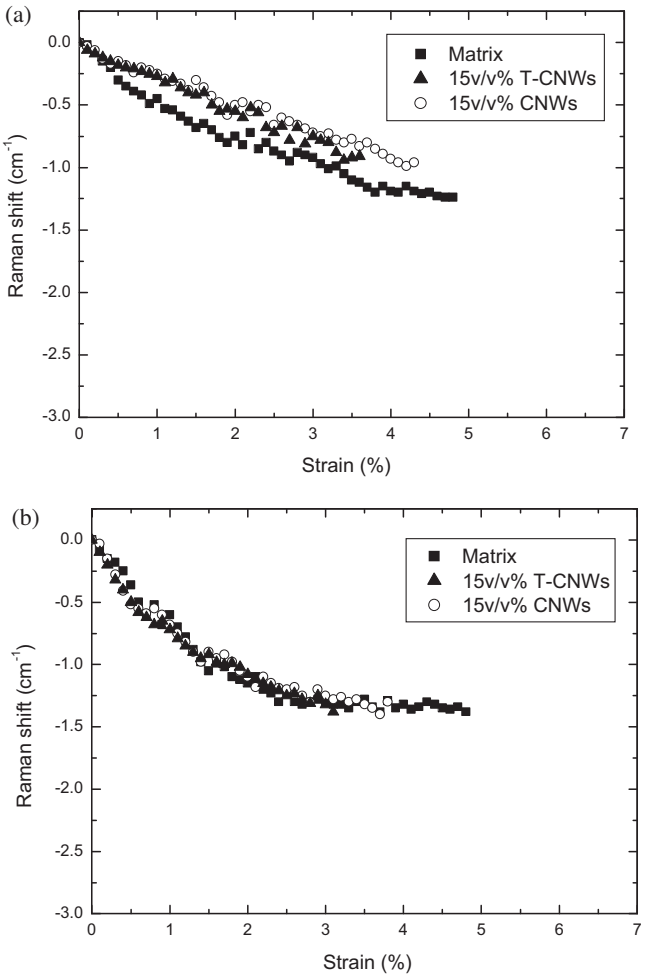

Fig. 8. Shifts in the peak positions of the Raman band initially located at ~895 cm^{-1} as a function of tensile deformation of all-cellulose nanocomposites and matrix materials produced using (a) LiCl/DMAc and (b) NaOH/urea solvent systems, reinforced with cellulose nanowhiskers from tunicates (T-CNWs) and cotton (CNWs) at a volume fraction of 15 v/v%.

which follows the mechanical properties data obtained for these materials. It is also noted that nanocomposites filled with T-CNWs achieve, on average, much higher band shift rates with respect to strain. This is expected since it is known that T-CNWs possess much higher aspect ratios than CNWs (Rusli et al., 2011), leading to enhanced stress-transfer and higher mechanical properties. In addition to this T-CNWs are assumed to have a higher stiffness compared to CNWs; values of ~140 GPa have been reported for T-CNWs (Iwamoto et al., 2009; Sturcova et al., 2005) compared to 50–105 GPa for CNWs (Rusli & Eichhorn, 2008). All datasets are observed to go through a maximum at 15 v/v%, corresponding with the maxima in strength and modulus observed for the samples' mechanical properties (see Tables 1 and 2). This shows the intimate relationship between the molecular deformation of the cellulose nanowhiskers, as a result of stress-transfer between the matrix and this reinforcing phase, and the mechanical properties of the nanocomposites themselves.

Table 3
Raman band shift rates with respect to strain for pure matrix material and all-cellulose nanocomposites produced using a LiCl/DMAc solvent system and a range of volume fractions (5–20 v/v%) of cellulose nanowhiskers derived from tunicates (T-CNWs) and cotton (CNWs). Data are obtained from a first derivative of a 3rd order polynomial fit to the positions of the Raman peak initially located at ~1095 cm^{-1} (see Fig. 6).

Sample	Band shift rate with respect to strain (% cm^{-1})
Matrix (LiCl/DMAc)	−0.3 ± 0.1
5 v/v% T-CNWs	−0.8 (0.04)
10 v/v% T-CNWs	−1.3 (0.04)
15 v/v% T-CNWs	−1.9 ± 0.1
20 v/v% T-CNWs	−1.5 ± 0.1
5 v/v% CNWs	−0.5 ± 0.1
10 v/v% CNWs	−0.7 (0.03)
15 v/v% CNWs	−0.9 ± 0.1
20 v/v% CNWs	−0.8 (0.04)

Table 4
Raman band shift rates with respect to strain for pure matrix material and all-cellulose nanocomposites produced using a NaOH/urea solvent system and a range of volume fractions (5–20 v/v%) of cellulose nanowhiskers derived from tunicates (T-CNWs) and cotton (CNWs). Data are obtained from a first derivative of a 3rd order polynomial fit to the positions of the Raman peak initially located at ~1095 cm^{-1} (see Fig. 7).

Sample	Band shift rate with respect to strain (% cm^{-1})
Matrix (NaOH/urea)	−0.2 ± 0.1
5 v/v% T-CNWs	−0.6 ± 0.1
10 v/v% T-CNWs	−1.0 (0.03)
15 v/v% T-CNWs	−1.5 (0.04)
20 v/v% T-CNWs	−1.3 ± 0.1
5 v/v% CNWs	−0.4 (0.04)
10 v/v% CNWs	−0.5 (0.03)
15 v/v% CNWs	−0.7 ± 0.1
20 v/v% CNWs	−0.6 ± 0.1

4. Conclusions

Structure property relationships between the crystallinities, mechanical properties and micromechanics of all-cellulose nanocomposites have been made. Two different matrix systems, and two different forms of cellulose nanowhisker, have been compared. It has been shown that cellulose nanowhiskers can reinforce matrices formed from LiCl/DMAc and NaOH/urea dissolved cellulose. A maximum reinforcement volume fraction of 15 v/v% has been found, after which mechanical properties have been observed to decrease. This decrease in mechanical properties also occurs at the same point as a plateau in the crystallinities found for the materials. Tunicate cellulose nanowhiskers are found to enhance the mechanical properties of the nanocomposites to a greater degree than cotton derived nanowhiskers. By following the molecular deformation of the nanowhiskers themselves, using a Raman spectroscopic technique, it is shown that this enhancement can be followed. Finally, it is thought that a combination of the LiCl/DMAc matrix system and the tunicate cellulose nanowhiskers yields the best mechanical properties.

Acknowledgement

The authors wish to thank the Royal Thai Government for a Ph.D. scholarship for T.P.

References

Abbott, A., & Bismarck, A. (2010). Self-reinforced cellulose nanocomposites. *Cellulose*, *17*, 779–791.
Atalla, R. H., & Dimick, B. E. (1975). Raman-spectral evidence for differences between conformations of cellulose-I and cellulose-II. *Carbohydrate Research*, *39*, C1–C3.
Cai, J., & Zhang, L. (2005). Rapid dissolution of cellulose in LiOH/urea and NaOH/urea aqueous solutions. *Macromolecular Bioscience*, *5*, 539–548.
Cai, J., & Zhang, L. (2006). Unique gelation behavior of cellulose in NaOH/urea aqueous solution. *Biomacromolecules*, *7*, 183–189.
Cai, J., Zhang, L. N., Zhou, J. P., Qi, H. S., Chen, H., Kondo, T., et al. (2007). Multifilament fibers based on dissolution of cellulose in NaOH/urea aqueous solution: Structure and properties. *Advanced Materials*, *19*, 821–825.
Capadona, J. R., Shanmuganathan, K., Tyler, D. J., Rowan, S. J., & Weder, C. (2008). Stimuli-responsive polymer nanocomposites inspired by the sea cucumber dermis. *Science*, *319*, 1370–1374.

Capadona, J. R., Van Den Berg, O., Capadona, L. A., Schroeter, M., Rowan, S. J., Tyler, D. J., et al. (2007). A versatile approach for the processing of polymer nanocomposites with self-assembled nanofibre templates. *Nature Nanotechnology*, *2*, 765–769.

Dagnon, K. L., Shanmuganathan, K., Weder, C., & Rowan, S. J. (2012). Water-triggered modulus changes of cellulose nanofiber nanocomposites with hydrophobic polymer matrices. *Macromolecules*, *45*, 4707–4715.

Dong, X. M., Kimura, T., Revol, J. F., & Gray, D. G. (1996). Effects of ionic strength on the isotropic-chiral nematic phase transition of suspensions of cellulose crystallites. *Langmuir*, *12*, 2076–2082.

Duchemin, B. J. C., Mathew, A. P., & Oksman, K. (2009). All-cellulose composites by partial dissolution in the ionic liquid 1-butyl-3-methylimidazolium chloride. *Composites Part A: Applied Science and Manufacturing*, *40*, 2031–2037.

Eichhorn, S. J. (2011). Cellulose nanowhiskers: Promising materials for advanced applications. *Soft Matter*, *7*, 303–315.

Eichhorn, S. J., Dufresne, A., Aranguren, M., Marcovich, N. E., Capadona, J. R., Rowan, S. J., et al. (2010). Review: Current international research into cellulose nanofibres and nanocomposites. *Journal of Materials Science*, *45*, 1–33.

Eichhorn, S. J., Hughes, M., Snell, R., & Mott, L. (2000). Strain induced shifts in the Raman spectra of natural cellulose fibers. *Journal of Materials Science Letters*, *19*, 721–723.

Eichhorn, S. J., Sirichaisit, J., & Young, R. J. (2001). Deformation mechanisms in cellulose fibres, paper and wood. *Journal of Materials Science*, *36*, 3129–3135.

Eichhorn, S. J., & Young, R. J. (2001). The Young's modulus of a microcrystalline cellulose. *Cellulose*, *8*, 197–207.

Eichhorn, S. J., & Young, R. J. (2003). Deformation micromechanics of natural cellulose fibre networks and composites. *Composites Science and Technology*, *63*, 1225–1230.

Eichhorn, S. J., & Young, R. J. (2004). Composite micromechanics of hemp fibres and epoxy resin microdroplets. *Composites Science and Technology*, *64*, 767–772.

Eichhorn, S. J., Young, R. J., & Yeh, W. Y. (2001). Deformation processes in regenerated cellulose fibers. *Textile Research Journal*, *71*, 121–129.

Elazzouzi-Hafraoui, S., Nishiyama, Y., Putaux, J. L., Heux, L., Dubreuil, F., & Rochas, C. (2008). The shape and size distribution of crystalline nanoparticles prepared by acid hydrolysis of native cellulose. *Biomacromolecules*, *9*, 57–65.

Favier, V., Chanzy, H., & Cavaille, J. Y. (1995). Polymer nanocomposites reinforced by cellulose whiskers. *Macromolecules*, *28*, 6365–6367.

Gierlinger, N., Schwanninger, M., Reinecke, A., & Burgert, I. (2006). Molecular changes during tensile deformation of single wood fibers followed by Raman microscopy. *Biomacromolecules*, *7*, 2077–2081.

Gindl, W., & Keckes, J. (2005). All-cellulose nanocomposite. *Polymer*, *46*, 10221–10225.

Gindl, W., & Keckes, J. (2007). Drawing of self-reinforced cellulose films. *Journal of Applied Polymer Science*, *103*, 2703–2708.

Gindl, W., Martinschitz, K. J., Boesecke, P., & Keckes, J. (2006). Structural changes during tensile testing of an all-cellulose composite by in situ synchrotron X-ray diffraction. *Composites Science and Technology*, *66*, 2639–2647.

Goffin, A. L., Raquez, J. M., Duquesne, E., Siqueira, G., Habibi, Y., Dufresne, A., et al. (2011). From interfacial ring-opening polymerization to melt processing of cellulose nanowhisker-filled polylactide-based nanocomposites. *Biomacromolecules*, *12*, 2456–2465.

Hamad, W. Y., & Eichhorn, S. (1997). Deformation micromechanics of regenerated cellulose fibers using Raman spectroscopy. *Journal of Engineering Materials and Technology: Transactions of the ASME*, *119*, 309–313.

Hamad, W. Y., Gurnagul, N., & Gulati, D. (2012). Analysis of fibre deformation processes in high-consistency refining based on Raman microscopy and X-ray diffraction. *Holzforschung*, *66*, 711–716.

Huber, T., Mussig, J., Curnow, O., Pang, S. S., Bickerton, S., & Staiger, M. P. (2012). A critical review of all-cellulose composites. *Journal of Materials Science*, *47*, 1171–1186.

Iwamoto, S., Kai, W. H., Isogai, A., & Iwata, T. (2009). Elastic modulus of single cellulose microfibrils from tunicate measured by atomic force microscopy. *Biomacromolecules*, *10*, 2571–2576.

Klemm, D., Heublein, B., Fink, H. P., & Bohn, A. (2005). Cellulose: Fascinating biopolymer and sustainable raw material. *Angewandte Chemie International Edition*, *44*, 3358–3393.

Klemm, D., Kramer, F., Moritz, S., Lindström, T., Ankerfors, M., Gray, D., et al. (2011). Nanocelluloses: A new family of nature-based materials. *Angewandte Chemie International Edition*, *50*, 5438–5466.

Kong, K., & Eichhorn, S. J. (2005a). Crystalline and amorphous deformation of process-controlled cellulose-II fibres. *Polymer*, *46*, 6380–6390.

Kong, K., & Eichhorn, S. J. (2005b). The influence of hydrogen bonding on the deformation micromechanics of cellulose fibers. *Journal of Macromolecular Science: Physics*, *B44*, 1123–1136.

Ma, H., Zhou, B., Li, H. S., Li, Y. Q., & Ou, S. Y. (2011). Green composite films composed of nanocrystalline cellulose and a cellulose matrix regenerated from functionalized ionic liquid solution. *Carbohydrate Polymers*, *84*, 383–389.

Marquardt, D. W. (1963). An algorithm for least-squares estimation of non-linear parameters. *Journal of the Society for Industrial and Applied Mathematics*, *11*, 431–441.

Mendez, J., Annamalai, P. K., Eichhorn, S. J., Rusli, R., Rowan, S. J., Foster, E. J., et al. (2011). Bioinspired mechanically adaptive polymer nanocomposites with water-activated shape-memory effect. *Macromolecules*, *44*, 6827–6835.

Mottershead, B., & Eichhorn, S. J. (2007). Deformation micromechanics of model regenerated cellulose fibre-epoxy/polyester composites. *Composites Science and Technology*, *67*, 2150–2159.

Nishino, T., & Arimoto, N. (2007). All-cellulose composite prepared by selective dissolving of fiber surface. *Biomacromolecules*, *8*, 2712–2716.

Nishino, T., Matsuda, I., & Hirao, K. (2004). All-cellulose composite. *Macromolecules*, *37*, 7683–7687.

Ou, R. X., Xie, Y. J., Shen, X. P., Yuan, F. P., Wang, H. G., & Wang, Q. W. (2012). Solid biopolymer electrolytes based on all-cellulose composites prepared by partially dissolving cellulosic fibers in the ionic liquid 1-butyl-3-methylimidazolium chloride. *Journal of Materials Science*, *47*, 5978–5986.

Pandey, J. K., Lee, S., Kim, H. J., Takagi, H., Lee, C. S., & Ahn, S. H. (2012). Preparation and properties of cellulose-based nano composites of clay and polypropylene. *Journal of Applied Polymer Science*, *125*, E651–E660.

Peetla, P., Schenzel, K. C., & Diepenbrock, W. (2006). Determination of mechanical strength properties of hemp fibers using near-infrared Fourier transform Raman microspectroscopy. *Applied Spectroscopy*, *60*, 682–691.

Pullawan, T., Wilkinson, A. N., & Eichhorn, S. J. (2010). Discrimination of matrix-fibre interactions in all-cellulose nanocomposites. *Composites Science and Technology*, *70*, 2325–2330.

Pullawan, T., Wilkinson, A. N., & Eichhorn, S. J. (2012). Influence of magnetic field alignment of cellulose whiskers on the mechanics of all-cellulose nanocomposites. *Biomacromolecules*, *13*, 2528–2536.

Qi, H. S., Cai, J., Zhang, L. N., & Kuga, S. (2009). Properties of films composed of cellulose nanowhiskers and a cellulose matrix regenerated from alkali/urea solution. *Biomacromolecules*, *10*, 1597–1602.

Qin, C., Soykeabkaew, N., Xiuyuan, N., & Peijs, T. (2008). The effect of fibre volume fraction and mercerization on the properties of all-cellulose composites. *Carbohydrate Polymers*, *71*, 458–467.

Ranby, B. G. (1949). Aqueous colloidal solutions of cellulose micelles. *Acta Chemica Scandinavica*, *3*, 649–650.

Revol, J. F., Bradford, H., Giasson, J., Marchessault, R. H., & Gray, D. G. (1992). Helicoidal self-ordering of cellulose microfibrils in aqueous suspension. *International Journal of Biological Macromolecules*, *14*, 170–172.

Rusli, R., & Eichhorn, S. J. (2008). Determination of the stiffness of cellulose nanowhiskers and the fiber-matrix interface in a nanocomposite using Raman spectroscopy. *Applied Physics Letters*, *93*, 033111.

Rusli, R., & Eichhorn, S. J. (2011). Interfacial energy dissipation in a cellulose nanowhisker composite. *Nanotechnology*, *22*, 325706.

Rusli, R., Shanmuganathan, K., Rowan, S. J., Weder, C., & Eichhorn, S. J. (2010). Stress-transfer in anisotropic and environmentally adaptive cellulose whisker nanocomposites. *Biomacromolecules*, *11*, 762–768.

Rusli, R., Shanmuganathan, K., Rowan, S. J., Weder, C., & Eichhorn, S. J. (2011). Stress transfer in cellulose nanowhisker composites-influence of whisker aspect ratio and surface charge. *Biomacromolecules*, *12*, 1363–1369.

Segal, L., Creely, J. J., Martin, A. E., & Conrad, C. M. (1959). An empirical method for estimating the degree of crystallinity of native cellulose using the X-ray diffractomete. *Textile Research Journal*, *29*, 786–794.

Soykeabkaew, N., Nishino, T., & Peijs, T. (2009). All-cellulose composites of regenerated cellulose fibres by surface selective dissolution. *Composites Part A: Applied Science and Manufacturing*, *40*, 321–328.

Soykeabkaew, N., Sian, C., Gea, S., Nishino, T., & Peijs, T. (2009). All-cellulose nanocomposites by surface selective dissolution of bacterial cellulose. *Cellulose*, *16*, 435–444.

Sturcova, A., Davies, G. R., & Eichhorn, S. J. (2005). Elastic modulus and stress-transfer properties of tunicate cellulose whiskers. *Biomacromolecules*, *6*, 1055–1061.

Tang, L. M., & Weder, C. (2010). Cellulose whisker/epoxy resin nanocomposites. *ACS Applied Materials & Interfaces*, *2*, 1073–1080.

Ten, E., Turtle, J., Bahr, D., Jiang, L., & Wolcott, M. (2010). Thermal and mechanical properties of poly(3-hydroxybutyrate-co-3-hydroxyvalerate)/cellulose nanowhiskers composites. *Polymer*, *51*, 2652–2660.

Tze, W. T. Y., O'Neill, S. C., Tripp, C. P., Gardner, D. J., & Shaler, S. M. (2007). Evaluation of load transfer in the cellulosic-fiber/polymer interphase using a micro-Raman tensile test. *Wood and Fiber Science*, *39*, 184–195.

van den Berg, O., Capadona, J. R., & Weder, C. (2007). Preparation of homogeneous dispersions of tunicate cellulose whiskers in organic solvents. *Biomacromolecules*, *8*, 1353–1357.

Wiley, J. H., & Atalla, R. H. (1987). Band assignments in the Raman-spectra of celluloses. *Carbohydrate Research*, *160*, 113–129.

Yousefi, H., Nishino, T., Faezipour, M., Ebrahimi, G., & Shakeri, A. (2011). Direct fabrication of all-cellulose nanocomposite from cellulose microfibers using ionic liquid-based nanowelding. *Biomacromolecules*, *12*, 4080–4085.

Yuan, H. H., Nishiyama, Y., Wada, M., & Kuga, S. (2006). Surface acylation of cellulose whiskers by drying aqueous emulsion. *Biomacromolecules*, *7*, 696–700.

Zhao, Q., Yam, R., Zhang, B. Q., Yang, Y. K., Cheng, X. J., & Li, R. (2009). Novel all-cellulose ecocomposites prepared in ionic liquids. *Cellulose*, *16*, 217–226.

Zhou, J. P., & Zhang, L. N. (2000). Solubility of cellulose in NaOH urea aqueous solution. *Polymer Journal*, *32*, 866–870.